The Journal of Immunology

Direct Antimicrobial Activity of IFN-β

Amber Kaplan, Michelle W. Lee, Andrea J. Wolf, Jose J. Limon, Courtney A. Becker, Minna Ding, Ramachandran Murali, Ernest Y. Lee, George Y. Liu, Gerard C. L. Wong and David M. Underhill

J Immunol 2017; 198:4036-4045; Prepublished online 14 April 2017;
doi: 10.4049/jimmunol.1601226
http://www.jimmunol.org/content/198/10/4036

The Journal of Immunology is published twice each month by The American Association of Immunologists, Inc., 1451 Rockville Pike, Suite 650, Rockville, MD 20852

Print ISSN: 0022-1767 Online ISSN: 1550-6606.

Direct Antimicrobial Activity of IFN-β

Amber Kaplan,*,[1] Michelle W. Lee,[†,‡,§,1] Andrea J. Wolf,[¶] Jose J. Limon,[¶] Courtney A. Becker,[¶] Minna Ding,[¶] Ramachandran Murali,[‖] Ernest Y. Lee,[†,‡,§] George Y. Liu,[‡,#] Gerard C. L. Wong,[†,‡,§,2] and David M. Underhill[¶,‖,2]

Type I IFNs are a cytokine family essential for antiviral defense. More recently, type I IFNs were shown to be important during bacterial infections. In this article, we show that, in addition to known cytokine functions, IFN-β is antimicrobial. Parts of the IFN-β molecular surface (especially helix 4) are cationic and amphipathic, both classic characteristics of antimicrobial peptides, and we observed that IFN-β can directly kill *Staphylococcus aureus*. Further, a mutant *S. aureus* that is more sensitive to antimicrobial peptides was killed more efficiently by IFN-β than was the wild-type *S. aureus*, and immunoblotting showed that IFN-β interacts with the bacterial cell surface. To determine whether specific parts of IFN-β are antimicrobial, we synthesized IFN-β helix 4 and found that it is sufficient to permeate model prokaryotic membranes using synchrotron x-ray diffraction and that it is sufficient to kill *S. aureus*. These results suggest that, in addition to its well-known signaling activity, IFN-β may be directly antimicrobial and be part of a growing family of cytokines and chemokines, called kinocidins, that also have antimicrobial properties. *The Journal of Immunology*, **2017, 198: 4036–4045.**

The type I IFNs are a pleiotropic family of cytokines. In particular, IFN-β was shown to be important in antiviral defense (1), antibacterial defense (2), cellular growth and apoptosis (3), and autoimmune disorders (4). There is strong purifying selection for IFN-β in the human genome, suggesting it is an important host defense molecule (5).

Staphylococcus aureus is a Gram-positive bacterium that naturally colonizes the nares of 30–50% of the world's population (6). *S. aureus* can also cause disease in humans, especially as a hospital-acquired infection. In recent years, antibiotic-resistant strains, such as methicillin-resistant *S. aureus*, have become increasingly prevalent (7). Consequently, it is becoming increasingly important that we understand how the host successfully combats *S. aureus* and how best to develop new therapies for treating methicillin-resistant *S. aureus* infections.

Antimicrobial peptides are a large and diverse family of antimicrobial molecules that exhibit potent antibacterial activity. Antimicrobial peptides are present throughout the mammalian body and are found in especially high concentrations on mucosal surfaces (8). Antimicrobial peptides are evolutionarily ancient, being conserved from invertebrates onward (9). Overall, antimicrobial peptides are characterized by a net positive charge (cationic) and segregated regions of polar and nonpolar residues (amphipathicity) (10). Antimicrobial peptides can selectively permeate bacterial membranes and kill via disruption of barrier function and/or binding to intracellular targets. The mechanism by which antimicrobial peptides permeate bacterial membranes is through the generation of the type of curvature topologically required for a variety of membrane-disruption processes, such as pore formation and blebbing, and is referred to as negative Gaussian curvature (NGC) (11, 12).

In this study, we found that IFN-β exhibits unexpected direct antimicrobial activity against *S. aureus*. Immunoblotting showed that IFN-β associates with the bacterial cell surface, and SYTOX Green staining suggested bacterial membrane permeabilization. This is suggestive of the activity of antimicrobial peptides. In fact, an *S. aureus* mutant that is specifically more susceptible to antimicrobial peptides was killed more efficiently by IFN-β compared with the wild-type (WT) strain. Parts of the IFN-β molecular surface (especially IFN-β helix 4) are cationic and amphipathic and have amino acid compositional preferences similar to α-helical antimicrobial peptides. We synthesized mouse and human IFN-β helix 4 and found, using synchrotron small-angle x-ray scattering (SAXS), that they have the ability to selectively disrupt bacterial, but not eukaryotic, model membranes. Together, these results suggest that IFN-β can be classified as a kinocidin, a growing family of cytokines and chemokines with inherent antimicrobial activi-

*Department of Microbiology, Immunology, and Molecular Genetics, University of California, Los Angeles, Los Angeles, CA 90095; [†]Department of Bioengineering, University of California, Los Angeles, Los Angeles, CA 90095; [‡]Department of Chemistry and Biochemistry, University of California, Los Angeles, Los Angeles, CA 90095; [§]California NanoSystems Institute, University of California, Los Angeles, Los Angeles, CA 90095; [¶]F. Widjaja Foundation Inflammatory Bowel and Immunobiology Research Institute, Cedars-Sinai Medical Center, Los Angeles, CA 90048; [‖]Research Division of Immunology, Cedars-Sinai Medical Center, Los Angeles, CA 90048; and [#]Division of Pediatric Infectious Diseases, Cedars-Sinai Medical Center, Los Angeles, CA 90048

[1]A.K. and M.W.L. are cofirst authors.

[2]G.C.L.W. and D.M.U. are cosenior authors.

ORCIDs: 0000-0003-1917-0512 (A.K.); 0000-0003-1613-9501 (M.W.L.); 0000-0002-8992-9267 (C.A.B.); 0000-0001-7497-8157 (M.D.); 0000-0002-8384-2793 (R.M.); 0000-0001-5144-2552 (E.Y.L.); 0000-0002-2989-658X (D.M.U.).

Received for publication July 15, 2016. Accepted for publication March 10, 2017.

This work was supported by grants from the National Institutes of Health (T32 AI007323 to A.K., R01 GM085796 to D.M.U., T32 AI089553-01 to A.J.W., R01 AI074832 to G.Y.L., and NSF-DMR-1411329 to M.W.L. and G.C.L.W.). E.Y.L. acknowledges support from the T32 Systems and Integrative Biology Training Grant at University of California, Los Angeles (T32GM008185) and the T32 Medical Scientist Training Program at University of California, Los Angeles (T32GM008042).

Address correspondence and reprint requests to Prof. David M. Underhill or Prof. Gerard C. L. Wong, Cedars-Sinai Medical Center, Davis Building D4063, 110 George Burns Road, Los Angeles, CA 90048 (D.M.U.) or University of California, Los Angeles, 420 Westwood Plaza, Engineering V, Los Angeles, CA 90095-1600 (G.C.L.W.). E-mail addresses: David.Underhill@csmc.edu (D.M.U.) or gclwong@seas.ucla.edu (G.C.L.W.)

The online version of this article contains supplemental material.

Abbreviations used in this article: DOPC, 1,2-dioleoyl-sn-glycero-3-phosphocholine; DOPE, 1,2-dioleoyl-sn-glycero-3-phosphoethanolamine; DOPG, 1,2-dioleoyl-sn-glycero-3-[phospho-*rac*-(1-glycerol)] (sodium salt); DOPS, 1,2-dioleoyl-sn-glycero-3-phospho-L-serine (sodium salt); hIFN-β, human IFN-β; LB, Luria broth; mIFN-β, mouse IFN-β; NGC, negative Gaussian curvature; P/L, peptide/lipid; SAXS, small-angle x-ray scattering; SUV, small unilamellar vesicle; THB, Todd–Hewitt broth; WT, wild-type.

ties (13, 14), and that its antimicrobial activity is cognate to that of antimicrobial peptides.

Materials and Methods

Bacterial strains and culture

S. aureus strains SA113, Newman, USA300, and Romero and *Staphylococcus epidermidis* were grown in Luria broth (LB) or Todd–Hewitt broth (THB). *Escherichia coli* DH5α, *Listeria monocytogenes*, *Pseudomonas aeruginosa*, *Salmonella typhimurium*, and *Bacillus subtilis* were grown in LB. Group B *Streptococcus* was grown in THB + 0.5% yeast extract. All bacteria were grown overnight at 37˚C with agitation, with the exception of Group B *Streptococcus*, which was cultured without agitation at 37˚C. Overnight bacterial cultures were subcultured and incubated until midlog was reached, which was determined to be OD_{600} = 0.4. Cultures were washed in sterile PBS and renormalized to OD_{600} = 0.4 in culture media.

Bacterial-killing assays

For killing assays using recombinant whole mouse IFN-β (mIFN-β; PBL Interferon), bacteria were grown as described above and resuspended in RPMI 1640 (Corning). One hundred–microliter reactions (bacteria + IFN-β or vehicle) were added to sterile 1.5-ml tubes. Tubes were incubated at 37˚C with shaking for 1, 3, or 24 h. After the specified incubation periods, 10-fold serial dilutions were plated on LB plates to quantify surviving CFU. We consistently noted significant differences in overall killing activity exhibited by different lots of recombinant mIFN-β.

For pH-specific killing assays using recombinant whole human IFN-β (hIFN-β; PBL Interferon), bacteria were grown as described above and resuspended in either 2 mM MES (pH 5.5) or 10 mM PIPES (pH 7.5), buffers that were previously shown to be good for assessing antimicrobial peptide activity at a variety of pHs (15). Two types of recombinant hIFN-β were tested from *E. coli* or CHO sources (PBL Interferon). One hundred–microliter reactions (bacteria + IFN-β or vehicle) were added to sterile 1.5-ml tubes. Tubes were incubated at 37˚C with shaking for 3 h. After specified incubation periods, 10-fold serial dilutions were plated on LB plates to quantify surviving CFU.

For killing assays using IFN-β helix 4 peptide or mutant IFN-β helix 4 peptide (synthesized by LifeTein or United Biosystems), bacteria were grown, as described above, and resuspended in 100 mM NaCl and 20 mM HEPES (pH 7.4) and, in some cases, were supplemented with 1% THB. One hundred–microliter reactions (bacteria + IFN-β helix 4 peptides or vehicle) were added to sterile 1.5-ml tubes, or 200-μl reactions were added to 96-well plates. Bacteria and treatments were incubated at 37˚C with shaking for designated amounts of time. After specified incubation periods, 10-fold serial dilutions were plated on agar plates of the proper media type for each strain to quantify surviving CFU.

SYTOX plate assay for bacterial survival

Bacteria were grown as described above and resuspended in 10 mM Tris-HCl (pH 7.5). One milliliter of *S. aureus* was incubated with 1 μM SYTOX Green (Thermo Fisher) in the dark at 37˚C with shaking for 20 min. Five microliters of each treatment (vehicle, 1 mM nigericin, or 5×10^3 U/ml mIFN-β) was added to a black 96-well plate. Ninety-five microliters of SYTOX Green–labeled bacteria was added to each 96-well plate. Fluorescence was read in a plate reader immediately and every 15 min thereafter at an excitation wavelength of 485 nm and an emission wavelength of 520 nm. The plate was continuously incubated at 37˚C with shaking in the dark when not being read.

SYTOX live-dead imaging of bacteria

Bacteria were grown, as described above, and resuspended in RPMI 1640 (Corning). One hundred microliters of *S. aureus* was incubated with vehicle, 1 mM nigericin, or 5×10^3 U/ml mIFN-β at 37˚C with shaking for 10 min. Bacteria were then pelleted, washed in PBS, resuspended in 10 mM Tris-HCl (pH 7.5), and incubated in the dark with 1 μg/ml DAPI and 0.5 μM SYTOX Green for 10 min. Labeled bacteria were applied to a slide by adding 2 μl and allowing it to dry (this process was repeated twice). Dried bacteria drops were covered in ProLong Gold (Thermo Fisher) mounting medium, and coverslips were added. Slides were dried for 1 h in the dark and then imaged by fluorescence microscopy. Images were quantified by enumeration of blue and green bacteria.

Immunoblotting for mIFN-β

S. aureus was incubated with increasing concentrations of mIFN-β. A total of 2×10^7 *S. aureus* in 100 μl of RPMI 1640 (Corning) in a 1.5-ml tube was incubated with 5 μl of vehicle or mIFN-β for 1 h. Bacteria were pelleted at maximum speed for 10 min on a microcentrifuge at room temperature. The supernatant was discarded, and bacteria were washed three times in PBS and processed for immunoblotting using a NuPAGE system (Thermo Fisher).

Washed bacterial pellets were lysed in NuPAGE LDS Sample Buffer (Thermo Fisher) by vortexing and incubation at room temperature for 5 min. Samples were boiled and loaded onto a 4–12% SDS-polyacrylamide gel. Proteins were transferred to polyvinylidene difluoride membranes (Millipore). Membranes were blocked with 5% BSA for 2 h at room temperature. Blots were incubated with primary Abs (rat anti-mouse IFN-β [RMMB-1; PBL Interferon] or anti-GAPDH [GA1R; MyBioSource]) at 1:1000 overnight at 4˚C. Infrared secondary Abs were used at 1:10,000, and the membrane was processed for use with the Odyssey Imaging System (all from LI-COR Biosciences).

Structural modeling of whole mouse and human IFN-β

The structural homology of mouse and human IFN-β was analyzed using PyMOL (The PyMOL Molecular Graphics System, Version 1.3, 2011; Schrodinger). The protein structure of each molecule was downloaded as a PDB file from the RCSB Protein Data Bank (http://www.pdb.org/pdb/home/home.do) and loaded into PyMOL. Further analyses were facilitated using the APBS software plug-in (http://www.poissonboltzmann.org) (16). Mouse and human IFN-β were analyzed for regions of positive and negative amino acid residues, and the resulting graphs show regions of the molecule that most likely contribute to overall positive charge.

Mouse and human IFN-β helix 4 peptides

Mouse (3175.8 m.w.) and human IFN-β helix 4 (2587.1 m.w.) peptides and mouse mutant IFN-β helix 4 (QASSTALQLASYYWAVQTYLALMKY) (2912.4 m.w.) were synthesized (≥95% purity; LifeTein or United Biosystems) with N-terminal acetylation and C-terminal amidation. WT peptides were solubilized in ultrapure water. Helical wheel projections were used to assess the proximity of positively charged amino acid residues in mouse and human IFN-β helix 4 peptides. Mutant IFN-β helix 4 was no longer soluble in water, so mutant helix 4 and a portion of WT helix 4 were solubilized in DMSO for comparison. In killing assays, DMSO was diluted to <0.5%, which was determined to have no effect on bacterial survival in a 3-h killing experiment.

Compositional comparison of mouse and human IFN-β helix 4 peptides with antimicrobial peptides

We compared the amino acid compositions of mouse and human IFN-β helix 4 peptides with the compositions of known antimicrobial peptides, which is a consequence of the required membrane curvature generation. A set of 1080 cationic antimicrobial peptide sequences was sourced from the antimicrobial peptide database (17) and analyzed using a procedure described previously (12, 18). We defined the average hydrophobicity of a given peptide, *j*, as:

$$\langle \text{hydrophobicity} \rangle_j \equiv \frac{1}{n} \sum_{i=1}^{n} \omega_i$$

where n is the number of amino acids in the peptide, and ω_i is the hydrophobicity of the ith amino acid in the peptide using the Eisenberg consensus hydrophobicity scale (19). The minimum and maximum <hydrophobicity> values within the set of antimicrobial peptide sequences were used to define a <hydrophobicity> range. This range was then divided into 100 equal bins, into which the peptides were partitioned. For m peptides in a given bin, we define:

$$\frac{N_K}{N_K + N_R} \equiv \frac{\sum_{j=1}^{m} (\text{number of K})_j}{\sum_{j=1}^{m} (\text{number of K})_j + (\text{number of R})_j}$$

where $N_K/(N_K + N_R)$ represents the ratio of the number of lysines/total number of lysines plus arginines. For each bin, $N_K/(N_K + N_R)$ versus <hydrophobicity> was plotted using MATLAB. Mouse and human IFN-β helix 4 peptides were analyzed and plotted using the same procedure.

To compare the hydrophobicities of mouse and human IFN-β helix 4 peptides with those of antimicrobial peptides, a histogram of <hydrophobicity> values for the set of antimicrobial peptides was constructed with 50 bins using MATLAB. The average hydrophobicities of mouse and

human IFN-β helix 4 peptides were superimposed over the antimicrobial peptide histogram.

SAXS experiments

Liposome preparation for x-ray measurements was carried out as follows. Lyophilized lipids (Avanti Polar Lipids) 1,2-dioleoyl-sn-glycero-3-[phospho-*rac*-(1-glycerol)] (sodium salt) (DOPG), 1,2-dioleoyl-sn-glycero-3-phospho-L-serine (sodium salt) (DOPS), 1,2-dioleoyl-sn-glycero-3-phosphoethanolamine (DOPE), and 1,2-dioleoyl-sn-glycero-3-phosphocholine (DOPC) were used without further purification to form small unilamellar vesicles (SUVs). Individual stock solutions of each lipid were prepared in chloroform at a concentration of 20 mg/ml. Lipid mixtures were prepared at specific molar ratios to yield each model membrane composition. Lipid mixture solutions were evaporated under N_2, desiccated overnight under vacuum, and then resuspended to a concentration of 20 mg/ml in aqueous 100 mM NaCl, 20 mM HEPES (pH 7.4) or 100 mM NaCl, 10 mM NaOAc (pH 5). Aqueous lipid solutions were incubated at 37°C overnight and then sonicated until clear. SUVs were obtained via extrusion of sonicated solution through a Nucleopore filter (Whatman) with 0.2-μm pores.

IFN-β helix 4 peptides and SUVs were mixed at specific peptide/lipid (P/L) molar ratios and hermetically sealed in quartz capillaries (Marktubes; Hilgenberg). All samples were prepared in 100 mM NaCl, 20 mM HEPES (pH 7.4) or 100 mM NaCl, 10 mM NaOAc (pH 5) and incubated at 37°C. SAXS experiments were performed at the Stanford Synchrotron Radiation Lightsource (beamline 4-2) using monochromatic x-rays with an energy of 9 keV. The scattered radiation was collected using a Rayonix MX225-HE detector (pixel size of 73.2 μm). Two-dimensional SAXS powder patterns were integrated using the Nika 1.50 (20) package for Igor Pro 6.31 and FIT2D.

SAXS data were analyzed by plotting the integrated scattering intensity I (Q) against Q using Origin Lab software. To determine the phase(s) present in each sample, the measured peak positions, Q_{meas}, were tabulated, and their ratios compared with those of the permitted reflections for different liquid-crystalline phases. The lattice parameter of each identified phase was calculated from the slope of the linear regression through points corresponding to the peaks, with each point having coordinates of Q_{meas} and the assigned reflection in terms of Miller indices h, k, and l. For a powder-averaged cubic phase, $Q = \frac{2\pi}{a}\sqrt{h^2+k^2+l^2}$, where a is the lattice parameter. Its average Gaussian curvature is defined as $\langle K\rangle = 2\pi\chi/a^2A_0$, where χ is the Euler characteristic, and A_0 is the surface area per cubic unit cell specific to each cubic phase.

Results

Mouse IFN-β is directly antimicrobial to S. aureus

In the course of studying the effects of IFN-β on host responses to *S. aureus* (21), we incubated the bacteria with a high dose of recombinant mIFN-β for 3 or 24 h. Surprisingly, after only 3 h we saw reduced survival of *S. aureus* (Fig. 1A). A dose curve revealed that growth inhibition of *S. aureus* started at concentrations of 500 U/ml IFN-β after 1 h of incubation (Fig. 1B). Such doses of IFN-β are not unusual in the literature and are thought to be biologically relevant (22–25). Having observed killing of *S. aureus* after incubation with IFN-β, we examined whether these antibacterial properties were effective against other species of bacteria. We also incubated *S. epidermidis* (Supplemental Fig. 1) with IFN-β and observed killing. However, when we incubated *E. coli* with increasing doses of IFN-β, we did not observe any inhibitory or killing effect (Fig. 1C).

To determine whether the killing effect of IFN-β was correlated with permeation of the bacterial cell membrane, we used a SYTOX Green assay. SYTOX Green dye is cationic and adheres

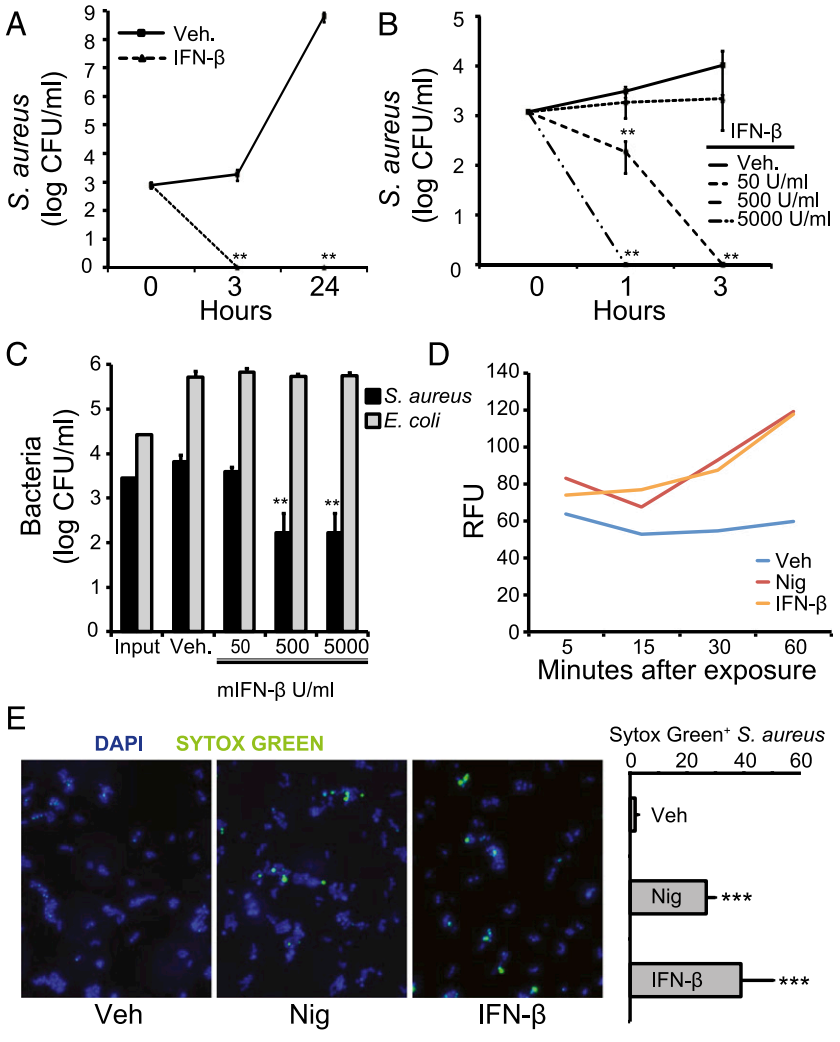

FIGURE 1. Mouse IFN-β kills *S. aureus*. (**A**) *S. aureus* were incubated with vehicle (Veh.) or 500 U/ml recombinant mIFN-β. Bacteria and treatments were incubated for 3 and 24 h. Remaining bacteria were serially diluted and plated for enumeration. (**B**) *S. aureus* were incubated with Veh. or mIFN-β (50, 500, or 5000 U/ml, which is equal to 0.0006, 0.006, or 0.06 μM). Bacteria were treated for 1 and 3 h. Remaining bacteria were serially diluted and plated for enumeration. (**C**) *S. aureus* or *E. coli* were incubated with Veh. or mIFN-β at the indicated concentrations for 3 h. Remaining bacteria were serially diluted and plated for enumeration. (**D**) *S. aureus* were incubated with SYTOX Green for 20 min. Bacteria were added to a 96-well plate preloaded with Veh, 1 mM nigericin (Nig), or 5×10^3 U/ml mIFN-β. The plate was imaged at 485/520 nm. Relative fluorescent units (RFU) are shown. (**E**) *S. aureus* were incubated with Veh, 1 mM Nig, or 5×10^3 U/ml mIFN-β for 10 min. Bacteria were stained with DAPI (blue) or SYTOX (green) and imaged (original magnification ×63) using a confocal microscope (left panels). Five separate images from each treatment were enumerated for blue versus green bacteria, and the results are plotted (right panel). Data are shown as mean ± SD. $^{**}p \leq 0.01$, $^{***}p \leq 0.001$, unpaired two-tailed t test.

to the negative surface of bacteria. The dye becomes fluorescent upon binding intracellular nucleic acids and, therefore, can be used to determine bacterial membrane disruption by external compounds (26). We incubated *S. aureus* with SYTOX Green and added IFN-β or the pore-forming toxin nigericin and monitored fluorescence initially and then every 15 min. We observed a marked increase in the fluorescent signal above vehicle when bacteria were exposed to IFN-β or nigericin (Fig. 1D), suggesting that IFN-β disrupts the bacterial membrane. We also used SYTOX Green to assess the effect of IFN-β and nigericin on *S. aureus* by confocal microscopy (Fig. 1E).

IFN-β antimicrobial activity correlates with cell-binding activity

There are many naturally occurring antimicrobial molecules found in mammals that aid in host defense (8). A large number of these molecules are antimicrobial peptides, which are commonly characterized by an overall positive charge and amphipathicity. The positive charge of antimicrobial peptides promotes their electrostatic attraction to the negative membranes of bacteria and less to host molecules, which are not as negatively charged (9). To determine whether IFN-β was capable of binding to *S. aureus*, we incubated bacteria with the cytokine and processed *S. aureus* for immunoblotting. We observed a dose-dependent association of IFN-β with the bacteria (Fig. 2A).

Multiple species of Gram-positive bacteria subvert host antimicrobial peptides by altering the lipoteichoic acids in their cell wall, effectively masking negative charges to result in a more positive overall charge (27). The *dlt* gene is one gene responsible for cell wall alterations that increase bacterial resistance to antimicrobial peptides. *S. aureus* strains in which the *dlt* gene has been deleted are more sensitive than WT strains to antimicrobial peptides but not to antibiotics with other modes of action (28). We incubated WT *S. aureus* and an isogenic mutant lacking the *dlt* gene with increasing concentrations of IFN-β. We observed increased killing of mutant bacteria lacking the *dlt* gene compared with WT, consistent with the hypothesis that IFN-β exhibits binding behavior cognate to those of antimicrobial peptides (Fig. 2B).

To investigate whether the antibacterial effects of IFN-β are intrinsic to the cytokine and are not due, for example, to a contaminant introduced during purification of the commercially prepared recombinant cytokine, we pretreated IFN-β with proteinase K to degrade the protein. Degradation diminished the ability of the cytokine to kill *S. aureus*, whereas killing was not lost after a similar incubation at 37°C (Fig. 2C). These results indicated that the IFN-β protein, or a portion of it, must be intact to function in an antimicrobial manner against *S. aureus*.

hIFN-β kills S. aureus *but only at acidic pH*

Having observed killing of *S. aureus* by mIFN-β, we investigated whether hIFN-β had similar properties. We incubated *S. aureus* with the same quantity of mouse or human IFN-β and quantified surviving bacteria. The results show that hIFN-β did not kill bacteria as well as mIFN-β (Fig. 3A). The nucleic acid and amino acid sequences of mouse and human IFN-β are homologous, and the tertiary structures of mouse and human IFN-β are quite similar, with a root-mean-square deviation > 0.4 (Fig. 3B). Thus, it was not immediately clear why they should have different killing abilities. Many antimicrobial peptides have improved function in an acidic pH environment (8, 29). Depending on the amino acid composition of the antimicrobial peptide, an acidic pH can contribute to a higher positive charge. There are many microenvironments in the body that are characterized by an acidic pH,

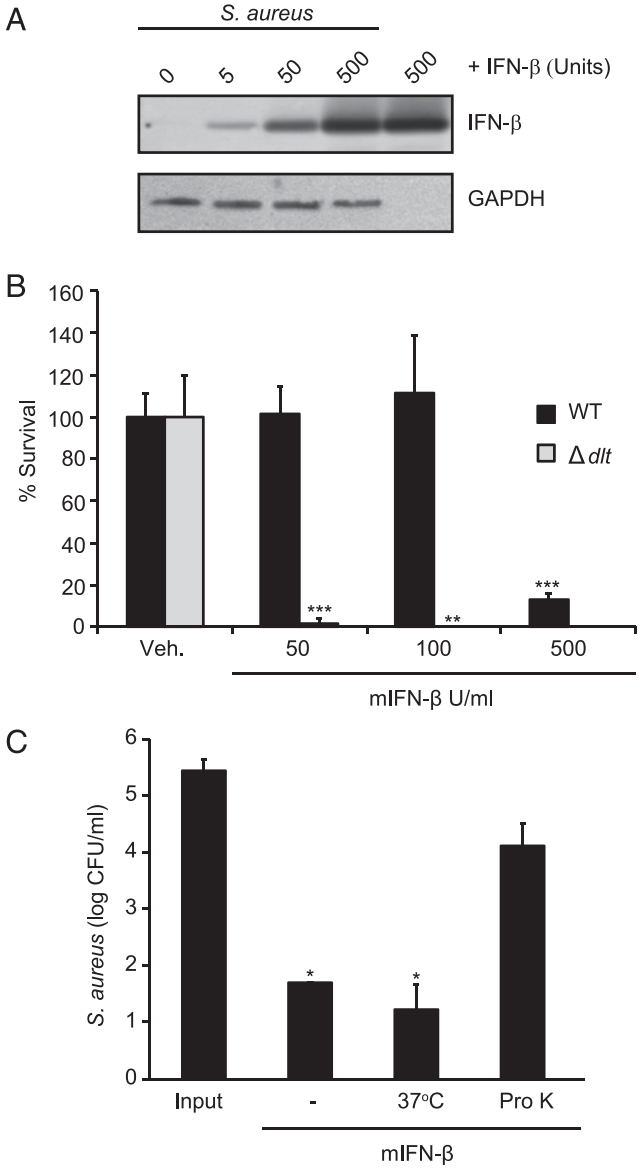

FIGURE 2. IFN-β has properties resembling antimicrobial peptides. (**A**) *S. aureus* were incubated with vehicle or the indicated units of mIFN-β for 1 h. Bacteria were washed twice to remove any mIFN-β not adhered to the bacterial surface. mIFN-β interacting with the *S. aureus* cell wall was detected by immunoblotting; 500 U mIFN-β was used as a positive control. Detection of bacterial GAPDH was used to control for the loading of equal amounts of bacteria. (**B**) WT or mutant *S. aureus* lacking the *dlt* gene (Δ*dlt*) were incubated with vehicle (Veh.) or mIFN-β at the indicated concentrations for 3 h. Remaining bacteria were serially diluted and plated for enumeration. (**C**) *S. aureus* were incubated with vehicle (Input), 5×10^2 U/ml mIFN-β (-), 5×10^2 U/ml mIFN-β incubated at 37°C for 60 min (37°C), or 5×10^2 U/ml mIFN-β incubated with proteinase K for 60 min (Pro K). Bacteria were incubated with variably treated mIFN-β for 3 h. Remaining bacteria were serially diluted and plated for enumeration. Data are shown as mean ± SD. $*p \leq 0.05$, $**p \leq 0.01$, $***p \leq 0.001$, unpaired two-tailed *t* test.

including the intracellular compartments of phagocytes (phagolysosomes), the surface of the skin, and abscesses. We evaluated the effect of pH on hIFN-β antimicrobial activity by incubating the protein with *S. aureus* at an acidic pH and observed a marked increase in bacterial killing at lower pH (Fig. 3C). We compared *S. aureus* survival after treatment with different concentrations of hIFN-β at an acidic pH of 5, relative to vehicle (Fig. 3D). These

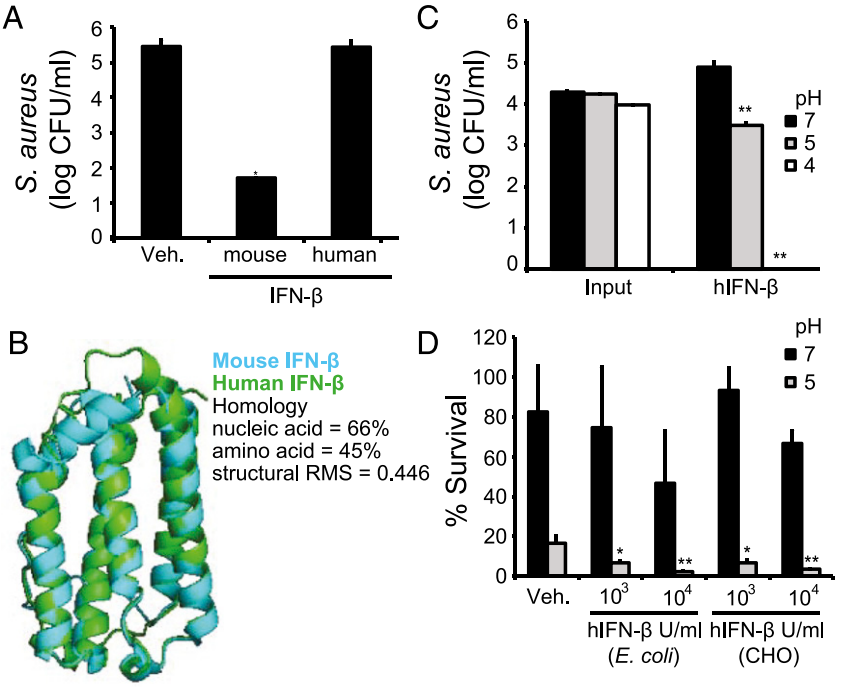

FIGURE 3. Human IFN-β kills *S. aureus* but only at low pH. (**A**) *S. aureus* were incubated with vehicle (Veh.), mIFN-β, or recombinant hIFN-β at the same concentration of 5×10^2 U/ml for 3 h. Remaining bacteria were serially diluted and plated for enumeration. (**B**) Mouse and human IFN-β were compared at the nucleic acid, amino acid, and structural levels. Structural root-mean-square deviation (RMS) is shown for overlay, which measures the average distance between atoms of superimposed mouse and human IFN-β. (**C**) *S. aureus* were incubated with vehicle (Input) or 5×10^3 U/ml hIFN-β at varying pHs for 3 h. Remaining bacteria were serially diluted and plated for enumeration. (**D**) *S. aureus* were incubated with Veh., hIFN-β produced in *E. coli*, or hIFN-β produced in CHO cells at the indicated concentrations. Bacteria were incubated with hIFN-β at neutral and low pH for 3 h. Remaining bacteria were serially diluted and plated for enumeration. Data are shown as the percentage of surviving bacteria based on initial CFU. Data are shown as mean ± SD. $*p \leq 0.05$, $**p \leq 0.01$, unpaired two-tailed *t* test.

results indicate that hIFN-β also has antimicrobial activity against *S. aureus* but at lower pH. Furthermore, recombinant hIFN-β produced in a bacterial (*E. coli*) or a mammalian (CHO cells) cell-expression system had killing activity at acidic pH (Fig. 3D), suggesting that posttranslational modifications are not required for antimicrobial activity.

Structural and compositional comparison of mouse and human IFN-β with antimicrobial peptides

Similar to many cytokines, the tertiary structure of IFN-β is a bundle of five α-helices, (helix 1–5, numbered sequentially from the N to C termini) (Fig. 4A). We compared the electrostatic potentials at neutral and acidic pH mapped onto space-filling models of mouse and human IFN-β (Fig. 4B). With cationic charge shown in blue, mIFN-β is highly positively charged at both pHs, whereas the net charge of hIFN-β doubles at acidic pH (Fig. 4B). In addition, charge calculations of all type I IFN family members for mouse and human showed a similar trend; many mouse type I IFNs are positively charged at neutral and acidic pH, whereas only a few human type I IFNs are positively charged at a neutral pH (Supplemental Fig. 2). Overall, the pH-dependent cationic charge of IFN-β may explain, in part, the killing ability that we observed experimentally.

To determine whether we could identify a specific region of IFN-β that confers killing activity, we examined the individual component helices (Fig. 4C) and calculated the net charge for each helix (Fig. 4D). For mouse and human IFN-β, the largest contribution to the net positive charge comes from the last two helices: 4 and 5 (Fig. 4D). In fact, when the individual charges of each amino acid were plotted, it was clear that the majority of positive residues were localized near the C terminus of the molecule in helices 4 and 5 (Fig. 4E). These charge plots also showed that, at an acidic pH, the net charge of the hIFN-β C-terminal region increases dramatically (Fig. 4E).

Although vastly diverse in sequence and structure, most antimicrobial peptides share several common features: they are generally short (<50 aa), have a net positive charge (+2 to +9), and have a substantial proportion (≥30%) of hydrophobic residues. The fundamental motif common among antimicrobial peptides is the ability to adopt an amphipathic secondary structure that clusters hydrophobic and cationic amino acids into distinct domains (30). Indeed, the cationic and amphipathic nature of antimicrobial peptides was found to be associated with their activity (30, 31).

The 21- and 17-residue-long regions corresponding to helix 4 of mouse and human IFN-β, respectively, have the highest proportion of cationic polar residues and hydrophobic residues relative to all helices present in the cytokine (Fig. 5A, 5B, Supplemental Fig. 3A). The two sequences also adopt facially amphipathic α-helical conformations, in which cationic and hydrophobic residues are segregated to opposite faces along the helical axis (Fig. 5A). These characteristics are similar to the structural motif common to a large class of antimicrobial peptides (32, 33).

We also observed similarities between the amino acid compositions of IFN-β helix 4 and those of antimicrobial peptide in general. In relation to the previously observed trend between $N_K/(N_K + N_R)$ (the ratio of the number of lysines/total number of lysines and arginines) and average peptide hydrophobicity based on the Eisenberg consensus scale (19) for 1080 cationic antimicrobial peptides from the antimicrobial peptide database (17), we found that mouse and human IFN-β helix 4 contain similar proportions of cationic and hydrophobic residues (Fig. 5C). In fact, their positions relative to the 1080 cationic antimicrobial peptide trendline (Fig. 5C) suggest a high compositional resemblance to antimicrobial peptides. Among the five helices of mouse and human IFN-β, helix 4 exhibited the greatest correspondence to the antimicrobial peptide trendline (Supplemental Fig. 3B). Moreover, when evaluating the amounts of hydrophobic residues independently, we found that the hydrophobicities of mouse and human IFN-β helix 4 also fall within the range of hydrophobicities of antimicrobial peptides (Fig. 5D, Supplemental Fig. 3C). In both comparisons, we included human LL-37, a well-characterized α-helical antimicrobial peptide (14), for reference. Taken together, these results suggest that mouse and human IFN-β helix 4 may interact with membranes in a manner similar to antimicrobial peptides.

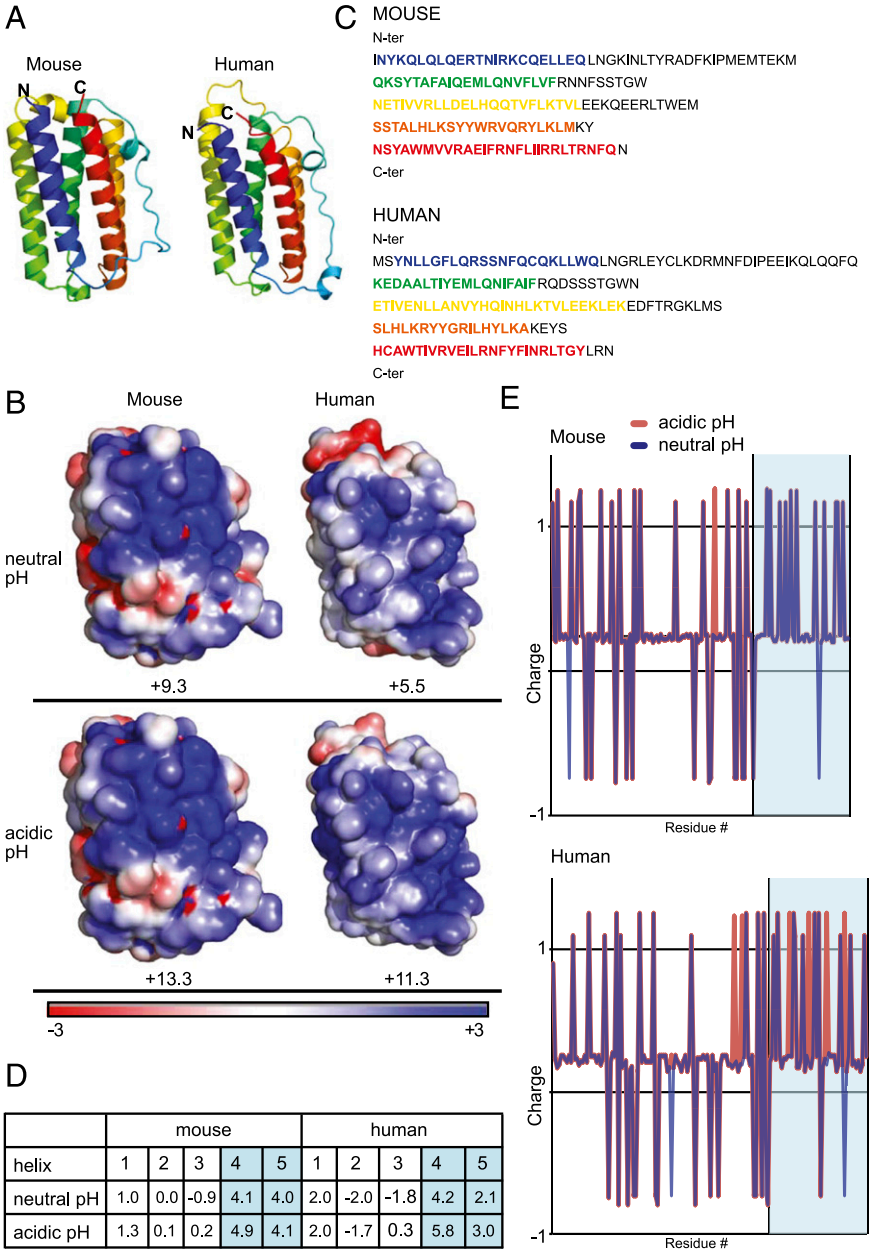

D

	mouse					human				
helix	1	2	3	4	5	1	2	3	4	5
neutral pH	1.0	0.0	-0.9	4.1	4.0	2.0	-2.0	-1.8	4.2	2.1
acidic pH	1.3	0.1	0.2	4.9	4.1	2.0	-1.7	0.3	5.8	3.0

FIGURE 4. Structural comparison of mouse and human IFN-β. (**A**) Mouse and human IFN-β ribbon structures are shown. N and C termini are labeled. The five α-helices are color coded, from the N to the C termini, as blue, green, yellow, orange, and red. (**B**) Mouse and human IFN-β electrostatic space filling models are shown for neutral pH (7) and acidic pH (5). Regions of positive charge are shown in blue, regions of neutral charge are shown in white, and regions of negative charge are shown in red. (**C**) Mouse and human IFN-β amino acid sequences are shown. The α-helices are color coded as in (A). (**D**) Charge was calculated for all five helices for mouse and human IFN-β. The high positive charge of helices 4 and 5 are highlighted in blue. (**E**) Mouse and human IFN-β amino acid plots were generated, showing the approximate charge of each amino acid residue. Values for neutral (blue) and acidic (red) pH are shown. The blue region shows helices 4 and 5.

Mouse IFN-β helix 4 induces membrane curvature in bacterial membranes and kills S. aureus

Earlier studies identified a strong correlation between the formation of NGC and antimicrobial peptide–induced membrane-destabilization mechanisms (11, 12, 34–37). NGC is also known as saddle-splay curvature, on which a surface curves upwards in one direction and downward in the perpendicular direction. NGC is topologically necessary for membrane-destabilizing processes, including pore formation, budding, and blebbing and, thus, is said to be the primary mode by which antimicrobial peptides compromise the barrier function of membranes (11, 12). For instance, NGC can be observed along the curved surface of a transmembrane pore (Fig. 6A).

We synthesized mouse and human IFN-β helix 4 peptides and used SAXS to quantitatively characterize the membrane curvature deformations that they induce. We systematically examined a range of membranes with varying lipid compositions, modeled from the differing compositions of bacterial and eukaryotic cell membranes (30, 33, 38, 39). For example, in bacterial membranes, phosphatidylglycerol and phosphatidylethanolamine are the main anionic and zwitterionic lipids, respectively. However, in eukaryotic membranes, phosphatidylserine is the primary anionic lipid, and phosphatidylcholine is the primary zwitterionic lipid. We prepared SUVs with a fixed anionic charge typical of bacterial membranes (20%) but with varying concentrations of phosphatidylethanolamine to represent bacterial membranes (DOPG/DOPE = 20:80) and more eukaryotic-like membranes (DOPG/DOPE/DOPC = 20:40:40 and DOPS/DOPC = 20:80). Additional lipid compositions (DOPG/DOPE/DOPC = 20:60:20 and DOPS/DOPE = 20:80) were included to assess the roles of phosphatidylethanolamine content and distinctions between the anionic lipids phosphatidylglycerol and phosphatidylserine, respectively. SUVs were incubated with mouse and human IFN-β helix 4 peptides at specific P/L molar ratios and pHs, and the resulting structures were characterized by SAXS.

SAXS spectra for two eukaryotic-like membrane compositions, DOPG/DOPE/DOPC = 20:40:40 and DOPS/DOPC = 20:80, incubated with the mouse and human IFN-β helix 4 peptides at P/L = 1:50

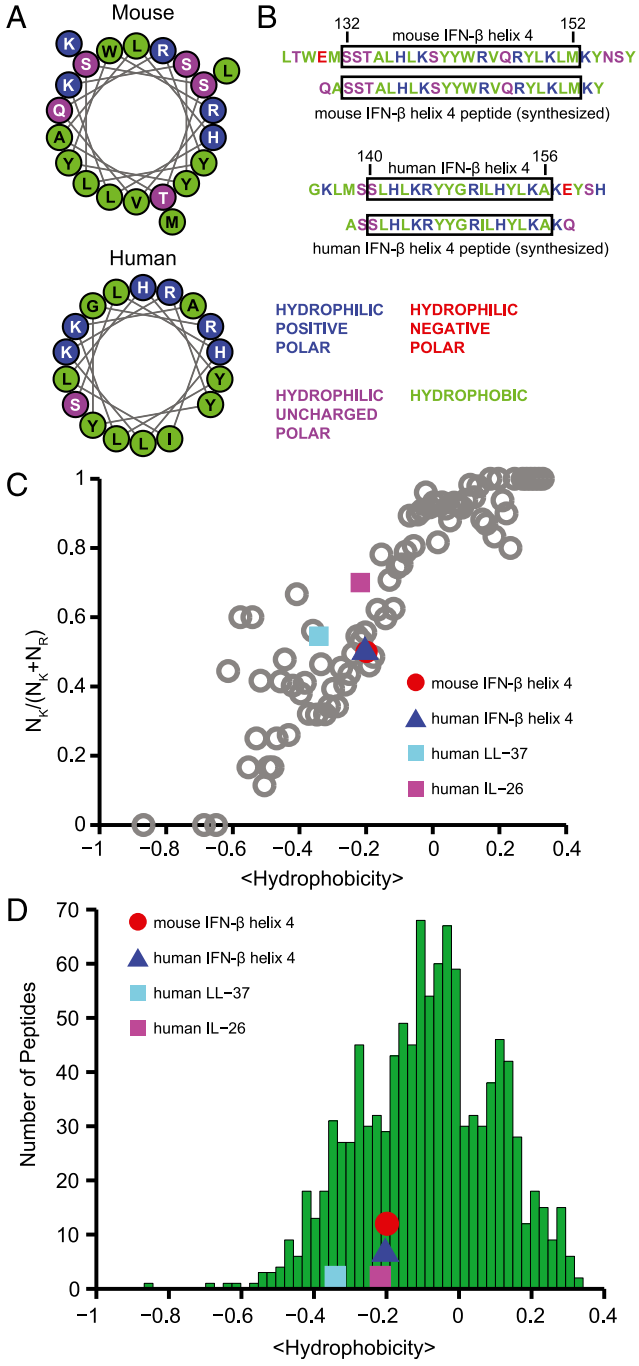

FIGURE 5. Mouse and human IFN-β helix 4 are similar to antimicrobial peptides. (**A**) Helical wheel projection plots of mouse and human IFN-β helix 4 sequences to illustrate their facial amphipathicity, which is characterized by the segregation of hydrophilic and hydrophobic residues to form two distinct faces along the helical axis. Positively charged hydrophilic residues are blue, negatively charged hydrophilic residues are red, uncharged hydrophilic residues are violet, and hydrophobic residues are green. (**B**) Mouse and human IFN-β helix 4 sequences; native sequences are shown alongside synthesized peptides. Helical regions are boxed. Residues are color coded as in (A). (**C**) Relationship between positively charged residues $[(N_K/(N_K + N_R)]$ and average peptide hydrophobicity for 1080 cationic antimicrobial peptides in the antimicrobial peptide database (gray circles). Mouse IFN-β helix 4, human IFN-β helix 4, human LL-37, and human IL-26 are plotted for comparison. (**D**) The hydrophobicity of IFN-β helix 4 is comparable to that of antimicrobial peptides. Histogram depicting the distribution of average hydrophobicities among 1080 cationic antimicrobial peptides in the antimicrobial peptide database (green bars) compared with the hydrophobicities of mouse IFN-β helix 4, human IFN-β helix 4, human LL-37, and human IL-26.

are shown in Fig. 6B. Synchrotron SAXS spectra for control SUVs exhibited characteristic features consistent with a single lipid bilayer (Supplemental Fig. 4A). Mouse and human IFN-β helix 4 peptides did not restructure either of the two eukaryotic membrane compositions at neutral pH, as shown by the form factors without correlation peaks. Similarly, hIFN-β helix 4 peptide at acidic pH (Fig. 6B) did not restructure DOPS/DOPC = 20:80 vesicles. For DOPG/DOPE/DOPC = 20:40:40, hIFN-β helix 4 peptide at an acidic pH induced a lamellar (L_α) phase ($d_{L\alpha} = 5.79$ nm) with correlation peaks at integral Q-ratios of 1:2:3. This result reveals intermembrane attraction without the generation of significant curvature. Overall, we find that mouse and human IFN-β helix 4 peptides do not induce NGC in eukaryotic-like membranes.

Fig. 6C shows SAXS spectra for prokaryotic-like membrane DOPG/DOPE = 20:80 with IFN-β helix 4 peptides at P/L = 1:50. Upon exposure to mIFN-β helix 4 peptide at neutral pH, the lipid vesicles underwent a structural transition, as revealed by correlation peaks with Q-ratios $\sqrt{2} : \sqrt{3} : \sqrt{4} : \sqrt{6} : \sqrt{8} : \sqrt{9} : \sqrt{10} : \sqrt{12}$, which indexed to a *Pn3m* "double-diamond" cubic (Q_{II}) lattice, with lattice parameter $a_{Pn3m} = 17.40$ nm (Supplemental Fig. 4B) and an average Gaussian curvature of $\langle K \rangle \approx -0.022$ nm^{-2} (see *Materials and Methods* for indexing procedures). In contrast, at neutral pH, hIFN-β helix 4 peptide did not restructure the DOPG/DOPE = 20:80 vesicles, as evidenced by a broad form factor characteristic of isolated spherical vesicles and the absence of correlation peaks (Fig. 6C). However, hIFN-β helix 4 peptide at an acidic pH resulted in two distinct sets of correlation peaks. One set of peaks has Q-ratios $\sqrt{2} : \sqrt{4} : \sqrt{6}$, which indexed to an *Im3m* Q_{II} phase with a lattice parameter $a_{Im3m} = 22.38$ nm and $\langle K \rangle \approx -0.021$ nm^{-2}. The second set of correlation peaks shows integral Q-ratios 1:2:3 consistent with an L_α phase of periodicity $d_{L\alpha} = 5.25$ nm, indicating intermembrane attraction. *Pn3m* and *Im3m* are bicontinuous cubic phases that consist of two nonintersecting aqueous regions separated by a lipid bilayer. The center of the bilayer traces a minimal surface characterized by NGC at every point. We find that mouse and human IFN-β helix 4 peptides are able to induce this membrane-destabilizing saddle-splay curvature in model bacterial membranes but not in model eukaryotic membranes. This type of behavior has been broadly observed for antimicrobial peptides, which suggests that the ability to selectively induce NGC is a general property of antimicrobial peptides (12). In fact, the NGCs induced by mouse and human IFN-β helix 4 peptides are quantitatively of similar magnitude to those of typical antimicrobial peptides (12). Moreover, we found that the generation of NGC by mouse and human IFN-β helix 4 peptides recapitulates the bactericidal activity of mouse and human IFN-β proteins, respectively, and the pH-dependent generation of NGC by hIFN-β helix 4 peptide tracks exactly with the pH-dependent killing activity by hIFN-β against *S. aureus*.

Similar to the results shown in Fig. 1 using the whole cytokine, we observed antimicrobial activity against *S. aureus* with mIFN-β helix 4 starting at nanomolar concentrations (Fig. 6D, 6E). To define the minimum bactericidal concentration of mIFN-β helix 4 against *S. aureus*, we quantified killing of *S. aureus* in response to 6.25–200 μM mIFN-β helix 4 (Fig. 6E). mIFN-β helix 4 exhibits a minimum bactericidal concentration of 12.5–25 μM, which is comparable to that of other antimicrobial peptides, such as LL-37. Taken together, these results demonstrate that mIFN-β helix 4 exhibits antimicrobial activity against *S. aureus* and are mutually consistent with our SAXS data. We found that the ability of mIFN-β helix 4 to generate NGC was similar to natural AMPs and tracked with its bactericidal activity, which together suggest

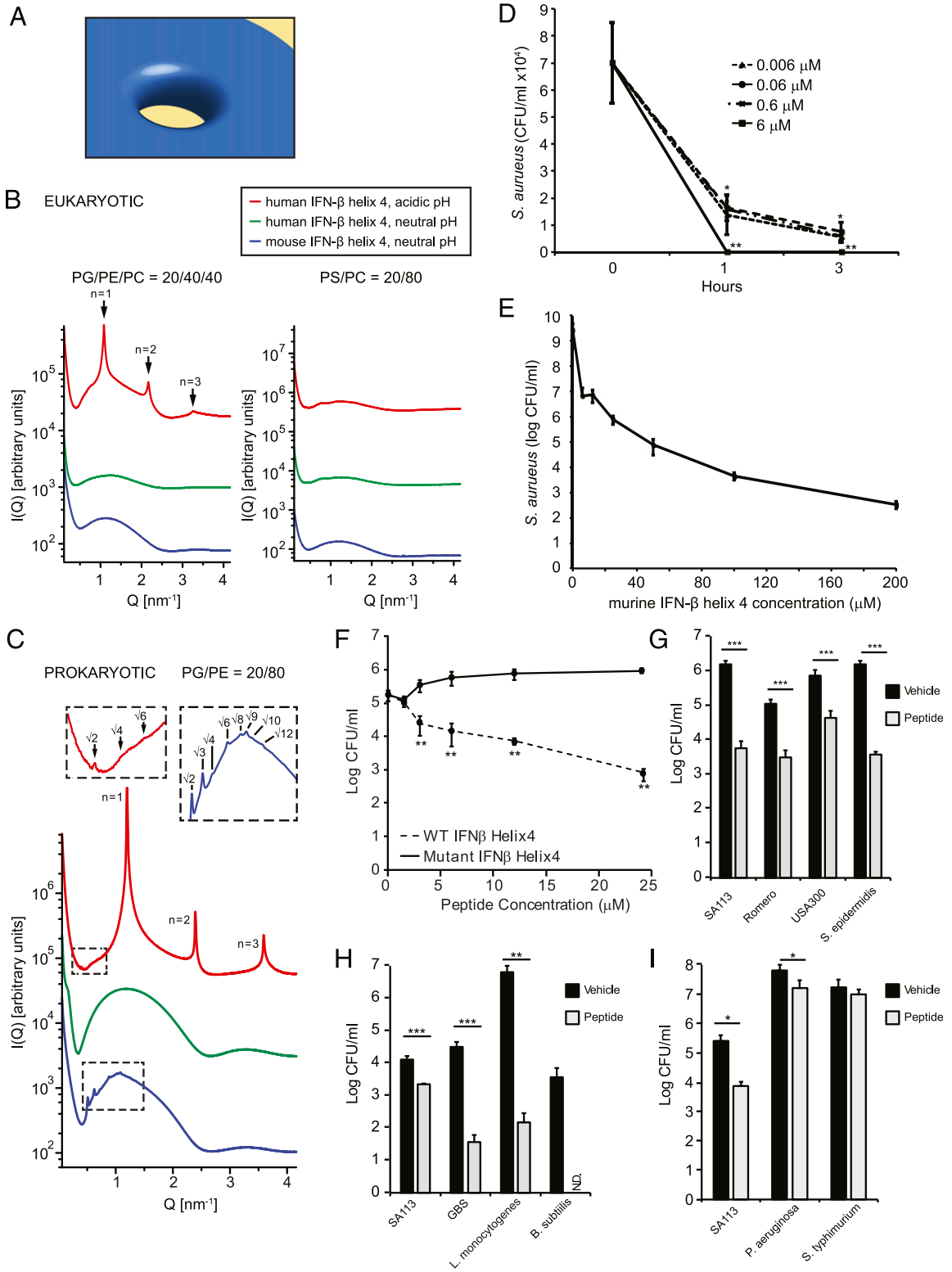

FIGURE 6. Mouse IFN-β helix 4 induces membrane curvature in bacterial membranes and kills S. aureus. (**A**) Model of NGC required for membrane-destabilization processes, such as pore formation by antimicrobial peptides. (**B**) IFN-β helix 4 does not generate NGC in eukaryotic-like membranes. SAXS spectra for mouse and human IFN-β helix 4 with eukaryotic model membranes DOPG/DOPE/DOPC = 20:40:40 and DOPS/DOPC = 20:80 at P/L = 1:50 molar ratio. (**C**) IFN-β helix 4 generates NGC in prokaryotic-like membranes. Mouse and human IFN-β helix 4 at P/L = 1:50 molar ratio incubated with prokaryotic model membrane, DOPG/DOPE = 20:80, generates cubic phases rich in NGC. Insets provide expanded views of cubic phase reflections. (**D**) *S. aureus* were incubated with vehicle or mIFN-β helix 4 at 0.006, 0.06, 0.6, and 6 μM. Bacteria and treatments were incubated for 1 or 3 h. Remaining bacteria were serially diluted and plated for enumeration. (**E**) *S. aureus* were incubated with vehicle or mouse IFN-β helix 4 at 6.25, 12.5, 25, 50, 100, and 200 μM. Bacteria and treatments were incubated for 3 h. Remaining bacteria were serially diluted and plated for enumeration. (**F**) WT and mutant IFN-β helix 4 peptides were incubated with 1×10^5 SA113 per milliliter in buffer + 1% THB for 3 h. Remaining bacteria were serially diluted and plated for enumeration. (**G–I**) Bacteria (1×10^5 per milliliter) were incubated with vehicle or 6 μM mIFN-β helix 4 peptide for 3 h at 37°C. Remaining bacteria were serially diluted and plated for enumeration. Data are shown as mean ± SD. *$p \leq 0.05$, **$p \leq 0.01$, ***$p \leq 0.001$, unpaired two-tailed t test. N.D., below limit of detection.

membrane permeation as at least one of its modes of antimicrobial activity.

To examine the specificity of mIFN-β helix 4's ability to kill bacteria, we generated a mutated version of helix 4 in which the charged amino acids hypothesized to be important for killing were neutralized. We observed that this mutated peptide was no longer able to kill *S. aureus* (Fig. 6F). When we incubated mIFN-β helix 4 with different strains of *Staphylococcus* bacteria, we found that it displays antimicrobial activity against multiple stains of *Staphylococcus* bacteria (Fig. 6G). In addition, the antimicrobial activity of mIFN-β was found to be effective against multiple strains of Gram-positive bacteria (Fig. 6H) but was significantly less effective against the Gram-negative strains of bacteria that we tested (Fig. 6I).

Discussion

We identified a previously unrecognized antimicrobial function of the cytokine IFN-β. We showed that mIFN-β is able to inhibit growth and directly kill *S. aureus*. In fact, the antibacterial activity of IFN-β resembles that of natural antimicrobial peptides in several respects, as demonstrated by its ability to bind and disrupt bacterial membranes. Examining this further, we found that the component helix 4 of IFN-β had structural and compositional properties, as well as net charge, that were similar to known antimicrobial peptides. Using SAXS, we then observed that, like typical antimicrobial peptides, synthesized mouse and human IFN-β helix 4 are capable of generating membrane NGC, the type of curvature required for membrane-disruption events. In fact, the generation of NGC by mouse and human IFN-β helix 4 peptides recapitulates the bactericidal activity of mouse and human IFN-β proteins, respectively, and the pH-dependent generation of NGC by human IFN-β helix 4 peptide tracks exactly with the pH-dependent killing activity by human IFN-β against *S. aureus.* Together, these results suggest that the antimicrobial activity that we observed experimentally with whole IFN-β is likely attributed, at least in part, to its component helix 4 having antimicrobial peptide–like properties. Thus, in addition to its well-documented cytokine activity, IFN-β has direct antimicrobial activity. Both activities are likely relevant to efficient clearance of bacterial infections, although their relative contributions likely depend on the type of bacteria, the site(s) of infection, and the duration of the infection. Future studies will be required to try to tease these roles apart.

Recent observations showed that proteins with antimicrobial peptide–like sequence trends exhibit antimicrobial activity (40), which is likely correlated with the ability of that protein surface to induce similar types of membrane curvatures as antimicrobial peptides. Another possibility is IFN-β degradation. Many antimicrobial peptides are secreted as proforms or even pre-pro forms, requiring cleavage events before the active peptide is released. For example, human cathelicidin is cleaved into the antimicrobial peptide LL-37 by serine proteases (10). Consistent with the degradation or cleavage hypothesis, we observed that a synthetic peptide consisting of helix 4 of IFN-β is sufficient to kill bacteria.

Kinocidins are defined as chemokines and cytokines that also have antimicrobial function, many of which function as antimicrobial peptides. A few notable examples include the α-chemokine family CXCL-1, -4, -6, -7, -8, -9, -10, and -14; the β-chemokine family CCL-1, -2, -5, and -8; and the cytokine IL-26 (13, 14). The findings in this study suggest that IFN-β is another member of the kinocidin family. Type I IFNs are increasingly recognized as important for host defense against bacteria. A protective role for this cytokine family was found for environmental and host-adapted bacterial pathogens (41). The new evidence presented in this article supports the notion that IFN-β has complementary antimicrobial activity and offers new insights into the multifunctional role and evolution of IFN-β in host defense.

Acknowledgments

We thank Dr. Jeff Miller for editing the manuscript.

Disclosures

The authors have no financial conflicts of interest.

References

1. Platanias, L. C. 2005. Mechanisms of type-I- and type-II-interferon-mediated signalling. *Nat. Rev. Immunol.* 5: 375–386.
2. Monroe, K. M., S. M. McWhirter, and R. E. Vance. 2010. Induction of type I interferons by bacteria. *Cell. Microbiol.* 12: 881–890.
3. Rizza, P., F. Moretti, and F. Belardelli. 2010. Recent advances on the immunomodulatory effects of IFN-α: implications for cancer immunotherapy and autoimmunity. *Autoimmunity* 43: 204–209.
4. González-Navajas, J. M., J. Lee, M. David, and E. Raz. 2012. Immunomodulatory functions of type I interferons. *Nat. Rev. Immunol.* 12: 125–135.
5. Zhang, S.-Y., S. Boisson-Dupuis, A. Chapgier, K. Yang, J. Bustamante, A. Puel, C. Picard, L. Abel, E. Jouanguy, and J.-L. Casanova. 2008. Inborn errors of interferon (IFN)-mediated immunity in humans: insights into the respective roles of IFN-α/β, IFN-γ, and IFN-λ in host defense. *Immunol. Rev.* 226: 29–40.
6. Wertheim, H. F., D. C. Melles, M. C. Vos, W. van Leeuwen, A. van Belkum, H. A. Verbrugh, and J. L. Nouwen. 2005. The role of nasal carriage in *Staphylococcus aureus* infections. *Lancet Infect. Dis.* 5: 751–762.
7. Miller, L. S., and J. S. Cho. 2011. Immunity against *Staphylococcus aureus* cutaneous infections. *Nat. Rev. Immunol.* 11: 505–518.
8. Ganz, T. 2003. Defensins: antimicrobial peptides of innate immunity. *Nat. Rev. Immunol.* 3: 710–720.
9. Peschel, A., and H.-G. Sahl. 2006. The co-evolution of host cationic antimicrobial peptides and microbial resistance. *Nat. Rev. Microbiol.* 4: 529–536.
10. Gallo, R. L., and L. V. Hooper. 2012. Epithelial antimicrobial defence of the skin and intestine. *Nat. Rev. Immunol.* 12: 503–516.
11. Schmidt, N. W., and G. C. L. Wong. 2013. Antimicrobial peptides and induced membrane curvature: geometry, coordination chemistry, and molecular engineering. *Curr. Opin. Solid State Mater. Sci.* 17: 151–163.
12. Schmidt, N. W., A. Mishra, G. H. Lai, M. Davis, L. K. Sanders, D. Tran, A. Garcia, K. P. Tai, P. B. McCray, Jr., A. J. Ouellette, et al. 2011. Criterion for amino acid composition of defensins and antimicrobial peptides based on geometry of membrane destabilization. *J. Am. Chem. Soc.* 133: 6720–6727.
13. Yount, N. Y., and M. R. Yeaman. 2012. Emerging themes and therapeutic prospects for anti-infective peptides. *Annu. Rev. Pharmacol. Toxicol.* 52: 337–360.
14. Meller, S., J. Di Domizio, K. S. Voo, H. C. Friedrich, G. Chamilos, D. Ganguly, C. Conrad, J. Gregorio, D. Le Roy, T. Roger, et al. 2015. T(H)17 cells promote microbial killing and innate immune sensing of DNA via interleukin 26. *Nat. Immunol.* 16: 970–979.
15. Tang, Y. Q., M. R. Yeaman, and M. E. Selsted. 2002. Antimicrobial peptides from human platelets. *Infect. Immun.* 70: 6524–6533.
16. Baker, N. A., D. Sept, S. Joseph, M. J. Holst, and J. A. McCammon. 2001. Electrostatics of nanosystems: application to microtubules and the ribosome. *Proc. Natl. Acad. Sci. USA* 98: 10037–10041.
17. Wang, G., X. Li, and Z. Wang. 2009. APD2: the updated antimicrobial peptide database and its application in peptide design. *Nucleic Acids Res.* 37: D933–D937.
18. Schmidt, N. W., A. Mishra, J. Wang, W. F. DeGrado, and G. C. Wong. 2013. Influenza virus A M2 protein generates negative Gaussian membrane curvature necessary for budding and scission. *J. Am. Chem. Soc.* 135: 13710–13719.
19. Eisenberg, D., N. W. Schmidt, T. C. Terwilliger, R. M. Weiss, G. C. Wong, and W. Wilcox. 1982. Hydrophobic moments and protein structure. *Faraday Symp. Chem. Soc.* 17: 109–120.
20. Ilavsky, J. 2012. Nika: software for two-dimensional data reduction. *J. Appl. Cryst.* 45: 324–328.
21. Kaplan, A., J. Ma, P. Kyme, A. J. Wolf, C. A. Becker, C. W. Tseng, G. Y. Liu, and D. M. Underhill. 2012. Failure to induce IFN-β production during *Staphylococcus aureus* infection contributes to pathogenicity. *J. Immunol.* 189: 4537–4545.
22. Inoue, M., P.-H. Chen, S. Siecinski, Q.-J. Li, C. Liu, L. Steinman, S. G. Gregory, E. Benner, and M. L. Shinohara. 2016. An interferon-β–resistant and NLRP3 inflammasome-independent subtype of EAE with neuronal damage. *Nat. Neurosci.* 19: 1599–1609.
23. Andrade, W. A., A. Firon, T. Schmidt, V. Hornung, K. A. Fitzgerald, E. A. Kurt-Jones, P. Trieu-Cuot, D. T. Golenbock, and P.-A. Kaminski. 2016. Group B *Streptococcus* degrades Cyclic-di-AMP to modulate STING-dependent type I interferon production. *Cell Host Microbe* 20: 49–59.
24. Mayer-Barber, K. D., B. B. Andrade, S. D. Oland, E. P. Amaral, D. L. Barber, J. Gonzales, S. C. Derrick, R. Shi, N. P. Kumar, W. Wei, et al. 2014. Host-directed therapy of tuberculosis based on interleukin-1 and type I interferon crosstalk. *Nature* 511: 99–103.

25. Teles, R. M., T. G. Graeber, S. R. Krutzik, D. Montoya, M. Schenk, D. J. Lee, E. Komisopoulou, K. Kelly-Scumpia, R. Chun, S. S. Iyer, et al. 2013. Type I interferon suppresses type II interferon-triggered human anti-mycobacterial responses. *Science* 339: 1448–1453.
26. Saar-Dover, R., A. Bitler, R. Nezer, L. Shmuel-Galia, A. Firon, E. Shimoni, P. Trieu-Cuot, and Y. Shai. 2012. D-alanylation of lipoteichoic acids confers resistance to cationic peptides in group B *streptococcus* by increasing the cell wall density. [Published erratum appears in 2012 *PLoS Pathog.* 8(11).] *PLoS Pathog.* 8: e1002891.
27. Peschel, A. 2002. How do bacteria resist human antimicrobial peptides? *Trends Microbiol.* 10: 179–186.
28. Peschel, A., M. Otto, R. W. Jack, H. Kalbacher, G. Jung, and F. Götz. 1999. Inactivation of the dlt operon in *Staphylococcus aureus* confers sensitivity to defensins, protegrins, and other antimicrobial peptides. *J. Biol. Chem.* 274: 8405–8410.
29. Yount, N. Y., and M. R. Yeaman. 2004. Multidimensional signatures in antimicrobial peptides. *Proc. Natl. Acad. Sci. USA* 101: 7363–7368.
30. Zasloff, M. 2002. Antimicrobial peptides of multicellular organisms. *Nature* 415: 389–395.
31. Hancock, R. E. W., and H.-G. Sahl. 2006. Antimicrobial and host-defense peptides as new anti-infective therapeutic strategies. *Nat. Biotechnol.* 24: 1551–1557.
32. Hancock, R. E., and R. Lehrer. 1998. Cationic peptides: a new source of antibiotics. *Trends Biotechnol.* 16: 82–88.
33. Brogden, K. A. 2005. Antimicrobial peptides: pore formers or metabolic inhibitors in bacteria? *Nat. Rev. Microbiol.* 3: 238–250.
34. Hu, K., N. W. Schmidt, R. Zhu, Y. Jiang, G. H. Lai, G. Wei, E. F. Palermo, K. Kuroda, G. C. Wong, and L. Yang. 2013. A critical evaluation of random copolymer mimesis of homogeneous antimicrobial peptides. *Macromolecules* 46: 1908–1915.
35. Xiong, M., M. W. Lee, R. A. Mansbach, Z. Song, Y. Bao, R. M. Peek, Jr., C. Yao, L. F. Chen, A. L. Ferguson, G. C. Wong, and J. Cheng. 2015. Helical antimicrobial polypeptides with radial amphiphilicity. *Proc. Natl. Acad. Sci. USA* 112: 13155–13160.
36. Schmidt, N. W., K. P. Tai, K. Kamdar, A. Mishra, G. H. Lai, K. Zhao, A. J. Ouellette, and G. C. L. Wong. 2012. Arginine in α-defensins: differential effects on bactericidal activity correspond to geometry of membrane curvature generation and peptide-lipid phase behavior. *J. Biol. Chem.* 287: 21866–21872.
37. Lee, M. W., S. Chakraborty, N. W. Schmidt, R. Murgai, S. H. Gellman, and G. C. L. Wong. 2014. Two interdependent mechanisms of antimicrobial activity allow for efficient killing in nylon-3-based polymeric mimics of innate immunity peptides. *Biochim. Biophys. Acta* 1838: 2269–2279.
38. van Meer, G., D. R. Voelker, and G. W. Feigenson. 2008. Membrane lipids: where they are and how they behave. *Nat. Rev. Mol. Cell Biol.* 9: 112–124.
39. Epand, R. M., and R. F. Epand. 2009. Lipid domains in bacterial membranes and the action of antimicrobial agents. *Biochim. Biophys. Acta* 1788: 289–294.
40. Realegeno, S., K. M. Kelly-Scumpia, A. T. Dang, J. Lu, R. Teles, P. T. Liu, M. Schenk, E. Y. Lee, N. W. Schmidt, G. C. Wong, et al. 2016. S100A12 is part of the antimicrobial network against *Mycobacterium leprae* in human macrophages. *PLoS Pathog.* 12: e1005705.
41. McNab, F., K. Mayer-Barber, A. Sher, A. Wack, and A. O'Garra. 2015. Type I interferons in infectious disease. *Nat. Rev. Immunol.* 15: 87–103.